ACSNANO
www.acsnano.org
ARTICLE

Reconfigurable Three-Dimensional Gold Nanorod Plasmonic Nanostructures Organized on DNA Origami Tripod

Pengfei Zhan,[†,#] Palash K. Dutta,[‡,#] Pengfei Wang,[‡,#] Gang Song,[§] Mingjie Dai,[∥] Shu-Xia Zhao,[§] Zhen-Gang Wang,[†] Peng Yin,[∥,⊥] Wei Zhang,[*,§] Baoquan Ding,[*,†,¶] and Yonggang Ke[*,‡]

[†]CAS Key Laboratory of Nanosystems and Hierarchical Fabrication, CAS Center for Excellence in Nanoscience, National Center for Nanoscience and Technology, Beijing 100190, China

[‡]Wallace H. Coulter Department of Biomedical Engineering, Georgia Institute of Technology and Emory University, Atlanta, Georgia 30322, United States

[§]Institute of Applied Physics and Computational Mathematics, Beijing 100088, China

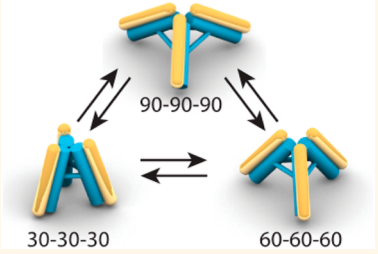
[∥]Wyss Institute for Biologically Inspired Engineering, Harvard University, Boston, Massachusetts 02115, United States

[⊥]Department of Systems Biology, Harvard Medical School, Boston, Massachusetts 02115, United States

[¶]University of Chinese Academy of Sciences, Beijing 100049, China

Supporting Information

ABSTRACT: **Distinct electromagnetic properties can emerge from the three-dimensional (3D) configuration of a plasmonic nanostructure. Furthermore, the reconfiguration of a dynamic plasmonic nanostructure, driven by physical or chemical stimuli, may generate a tailored plasmonic response. In this work, we constructed a 3D reconfigurable plasmonic nanostructure with controllable, reversible conformational transformation using bottom-up DNA self-assembly. Three gold nanorods (AuNRs) were positioned onto a reconfigurable DNA origami tripod. The internanorod angle and distance were precisely tuned through operating the origami tripod by toehold-mediated strand displacement. The transduction of conformational change manifested into a controlled shift of the plasmonic resonance peak, which was studied by dark-field microscopy, and agrees well with electrodynamic calculations. This new 3D plasmonic nanostructure not only provides a method to study the plasmonic resonance of AuNRs at prescribed 3D conformations but also demonstrates that DNA origami can serve as a general self-assembly platform for constructing various 3D reconfigurable plasmonic nanostructures with customized optical properties.**



KEYWORDS: *DNA origami, DNA nanotechnology, plasmonic nanostructure, gold nanorod, dark-field scattering spectroscopy*

Plasmonic metamaterials are artificial architectures, whose optical properties rise from precise arrangement of micro- or nanoscale metallodielectric building blocks.[1] Various plasmonic metamaterials have been fabricated and show a range of distinct optical properties, such as Fano resonance,[2] circular dichroism,[3] and enhanced nonlinear optical properties.[4] Conventional fabrications of plasmonic metamaterials are often achieved by top-down techniques, which are limited by throughput, resolution, and capability to fabricate 3D reconfigurable plasmonic nanostructures.[5] The evolvement of structural DNA nanotechnology provides an efficient solution to this challenge. In particular, with the DNA origami technique,[6,7] many complex 3D DNA nanostructures have been constructed, such as closely packed 3D shapes,[8,9] hollow DNA boxes,[10,11] 3D shapes with curvatures,[12] and wireframe nanostructures with multiarm junction vertices.[13−16] Furthermore, DNA nanostructures, serving as templates with spatially addressable binding sites, have demonstrated the power to organize a variety of molecules or nanoscale objects, such as chromophores,[17,18] quantum dots,[19,20] carbon nanotubes,[21] proteins,[22] or metallic nanoparticles,[23−29] into well-defined geometries to achieve desired functions.

DNA origami has been used to fabricate two- or three-dimensional photonic nanostructures effectively.[26,30−37] Nanostructures based on high-order anisotropic nanoscale building blocks, such as gold nanorods (AuNRs), generate optical properties that can be tuned by many geometric features, including nanorod size and aspect ratio and inter-rod distance and angle.[38] Nonetheless, despite progress on geometrical control over architectures of DNA origami templated

Received: October 11, 2016
Accepted: January 5, 2017
Published: January 5, 2017

Downloaded via UNIV OF CALIFORNIA DAVIS on November 16, 2023 at 23:25:22 (UTC).
See https://pubs.acs.org/sharingguidelines for options on how to legitimately share published articles.

© 2017 American Chemical Society

DOI: 10.1021/acsnano.6b06861
ACS Nano 2017, 11, 1172−1179

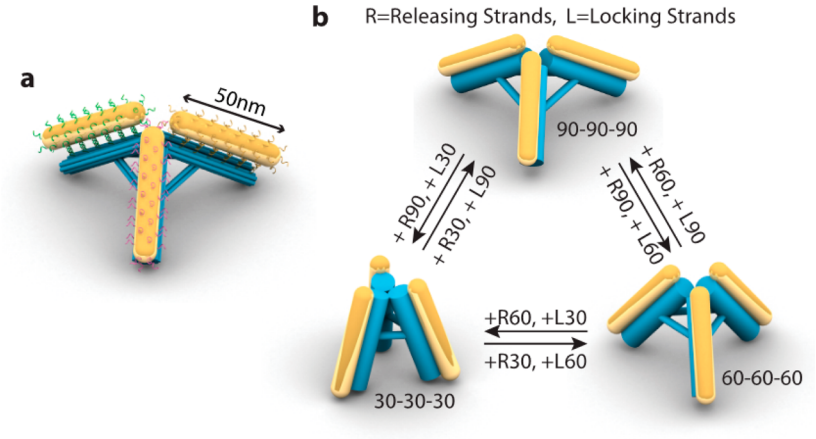


Figure 1. Schematic illustration of the reconfigurable DNA origami tripod with gold nanorods. (a) Diagram of gold nanorods assembled on the DNA tripod. Each arm is 50 nm in length. Two parallel double helices, denoted as strut, control the angle between the DNA arms. The length of the strut determines the interarm angle. (b) Toehold-mediated strand displacement reaction is used to tune the angle between the arms. Sets of releasing strands (R) and locking strands (L) are employed stepwise to change the angle between the DNA arms.

AuNRs,[33,39−42] it remains challenging to tune the inter-rod angles simultaneously within 3D reconfigurable systems containing multiple AuNRs. It is of great importance in the field of optical information conduction and storage to increase the complexity of AuNR-based reconfigurable photonic nanostructures, as it is evident that the functionality of the signal-transition network is upgraded as the number of AuNRs increases.[43] While DNA origami has been used to realize the reconfiguration of nanostructures containing two gold nanorods,[33] reconfigurable 3D plasmonic systems with three or more AuNRs have not been reported. Here, we demonstrated the construction and the reconfiguration of tripod-shaped plasmonic nanostructures consisting of three AuNRs. The reconfigurable AuNR plasmonic nanostructure was achieved by assembling AuNRs on the arms of a DNA origami tripod (Figure 1a). The optical responses from the discrete plasmonic AuNR-tripod, which adopted different conformations *via* toehold-mediated strand displacement reactions (Figure 1b), were observed in the visible range.

RESULTS AND DISCUSSION

Reconfigurable DNA Origami Tripod. The reconfigurable DNA origami tripod is modified from a published version.[13] The tripod contains three ∼50 nm arms (Figure 2a). Each arm contains 14 DNA duplexes (previous version has 16 duplexes per arm) packed on a honeycomb lattice to accommodate curvature of the AuNRs (see Methods for details). This design allowed incorporation of 12 single-stranded handle strands along the two central duplexes on each arm to capture AuNRs (Figure 2a). The interarm angle was controlled by adjusting the lengths of connecting struts composed of two parallel double helices.[13] Three sets of "locking" strands (L30, L60, L90) were utilized to create interarm angles of ∼30°, ∼60°, and ∼90° (Figure 2b). In addition, each locking strand has a different 14-base toehold that enables removal of the locking strand. Thus, the reversible reconfiguration of the tripod was realized by adding complementary "releasing" strands (R30, R60, R90) to change a strut to a "no locking" state, followed by addition of locking strands to relock the tripod to another conformation. The tripod conformations were named in accordance with the interarm angles (*e.g.*, 30−30−30 corresponds to the conformation with equal 30° angles between arms).

First, three tripods, 30−30−30, 60−60−60, and 90−90−90, were created separately by folding a 7560-nucleotide-long M13-based single-stranded DNA scaffold[44] using ∼180 short "staple" oligonucleotides. The tripods were then verified by gel electrophoresis (Figure 2c), which revealed that the tripod with smaller angles has higher mobility than the tripod with larger angles due to its more compact conformation. In addition, we also demonstrated one-step conversion from any one conformation (*e.g.*, 30−30−30) to the other two conformations (Figure 2c). The 30−30−30, the 60−60−60, and the 90−90−90 tripods were purified from agarose gel and subjected to subsequent transmission electron microscopy (TEM) imaging, which unambiguously confirmed the designed conformations (Figure 2d). The angles between two arms were measured from the images (Figure 2e). The 30−30−30 tripod, the 60−60−60 tripod, and the 90−90−90 tripod gave average interarm angles of 29 ± 4° (standard deviation, 54 counts), 53 ± 6° (standard deviation, 98 counts), and 85 ± 6° (standard deviation, 115 counts), respectively. To test the conformation change, the 30−30−30 tripod, 60−60−60 tripod, and 90−90−90 tripod were first converted, by adding "releasing strands", to the "no locking" tripod, which showed higher mobility in agarose gel, due to flexibility of the "no locking" tripod (Figures 2c, S1). Then the "no locking" tripods were transformed to the 30−30−30 tripod, the 60−60−60 tripod, and the 90−90−90 tripod by adding corresponding "locking" strands. These transformed tripods exhibited same mobility as the tripods assembled in one-pot reactions (Figures 2c, S2, and S3), suggesting reliable tripod reconfiguration, which was further confirmed by TEM imaging (Figure S4). Asymmetric tripods can be generated by tuning interarm angles independently. To demonstrate this, we converted the 60−60−60 tripod to a 30−60−60 tripod and a 60−60−90 tripod, and the 90−90−90 tripod to a 30−90−90 tripod and a 60−90−90 tripod. Both gel electrophoresis (Figure 2f) and TEM images (Figure 2g) confirmed the successful conversion to these asymmetric tripods.

To study the tripod configuration upon surface attachment in the "native" hydrated environment, we performed DNA-PAINT super-resolution imaging[13,45,46] on three sets of symmetric tripod configurations (30−30−30, 60−60−60, and 90−90−90) (see Methods for details). The DNA-PAINT

DOI: 10.1021/acsnano.6b06861
ACS Nano 2017, 11, 1172−1179

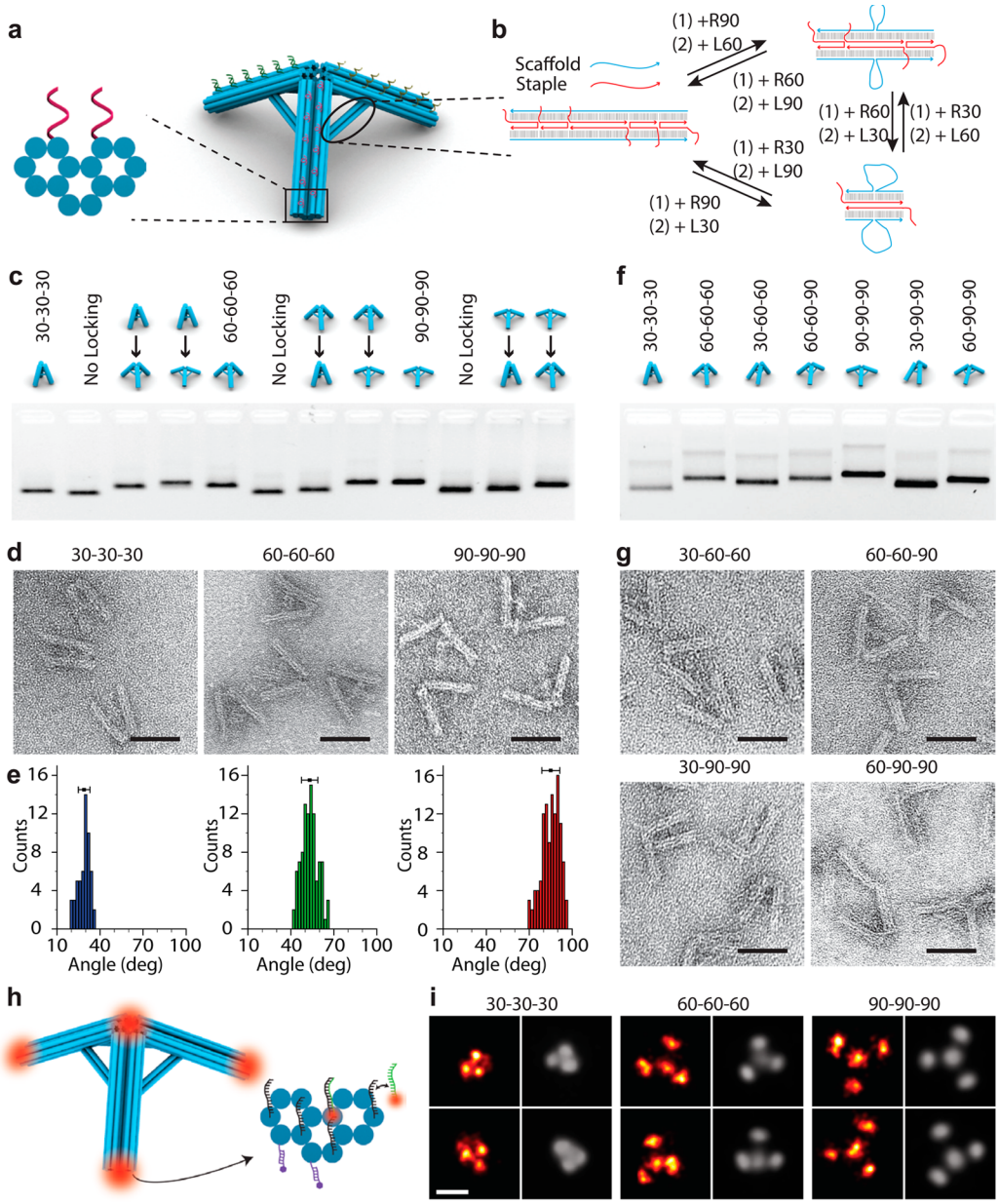


Figure 2. Reconfiguration of DNA origami tripods. (a) Design diagram of a tripod. Each arm is constituted with 14 parallel double helices with each cylinder representing a DNA double helix. The angle between the arms is determined by the strut length. (b) Details of the strut design. Each strut is composed of scaffold and staples with a 14-base-long toehold. Interarm angles could be tuned *via* using corresponding releasing and locking strands. (c) Agarose gel electrophoresis of tripods with various configurations. Each configuration of the tripods (30−30−30, 60−60−60, and 90−90−90) could be converted to the other two configurations. Lanes named "No Locking" represent the tripods after adding corresponding releasing strands. (d) TEM images of tripods with configurations of 30−30−30, 60−60−60, and 90−90−90. (e) Corresponding angle distribution histogram. The black square on each histogram reflects the mean value, and the horizontal line shows the standard deviation. (f) Agarose gel electrophoresis of tripods with asymmetric angles formed from purified 60−60−60 and 90−90−90 tripods. (g) TEM images of tripods with asymmetric angles. (h) Illustration of the DNA-PAINT imaging: a DNA origami tripod is decorated with single-stranded extensions (docking strand, black) on three feet and the vertex. Complementary Cy3b dye-modified strands (imager strand, green) transiently bind to docking strands. Biotinylated strands (purple, 2 on each foot) immobilize the tripod structures to the streptavidin-coated glass surface for fluorescence imaging. (i) DNA-PAINT super-resolution reconstruction of tripods. For each structure the left panel shows the super-resolution-rendered images (colored), and the right panel shows the single-particle ensemble analysis image (gray). Scale bars: 50 nm.

method uses transient programmable hybridization between short single-stranded oligonucleotide extensions (docking strands, black strand) on the target and complementary dye-conjugated strands (imager strands, green strand) in the solution to create effective "blinking" for localization-based super-resolution microscopy (Figure 2h). We included docking strands at the vertex and three feet of the tripods and anchored the tripod onto the substrate through a specific bridge between biotin on the feet (Figure 2h, purple, 2 biotins on each foot) and streptavidin on the substrate surface. Upon DNA-PAINT imaging and super-resolution reconstruction, a triangular pattern with a center point was observed for all configurations

DOI: 10.1021/acsnano.6b06861
ACS Nano 2017, 11, 1172−1179

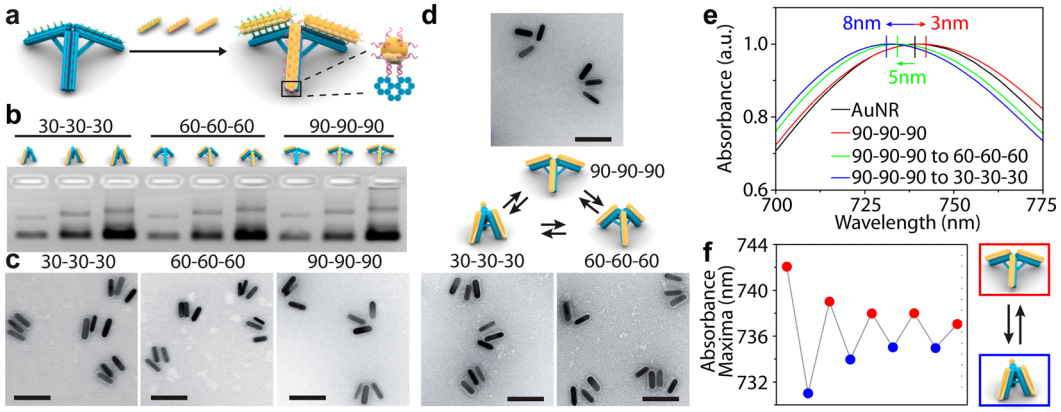


Figure 3. Construction of reconfigurable plasmonic AuNR-tripods. (a) Scheme of AuNR-tripod conjugation. The AuNR capturing strands (15 bases long) on each arm of the tripod have different sequences, highlighted with red, green, and yellow color. A total of 12 capturing strands are placed on each arm of the tripod. (b) Agarose gel electrophoresis of tripods with one, two, and three AuNRs at configurations of 30−30−30, 60−60−60, and 90−90−90. (c) TEM images of AuNR-tripod in three configurations. (d) Reconfiguration of AuNR-tripod. TEM images of the AuNR-tripods with configurations of 90−90−90 (top), 30−30−30 (bottom-left, converted from the 90−90−90 AuNR-tripod), and 60−60−60 (bottom-right, converted from the 90−90−90 AuNR-tripod). (e) Absorbance spectra of free-DNA-conjugated AuNR (black line), AuNR-assembled 90−90−90 tripod (red line), and 30−30−30 (blue line) and 60−60−60 (green line) tripods converted from the 90−90−90 tripod with an absorbance peak shift in comparison to DNA-conjugated AuNR (black line). (f) Absorbance maxima shifts showing reconfiguration cycling between the 90−90−90 and the 30−30−30 AuNR-tripods. Scale bars: 100 nm.

and with increasing vertex-to-vertex distances (Figure 2i, left columns). Single-particle ensemble analysis revealed a large population of regular triangular patterns with a centered middle point and designed vertex-to-vertex distance, as well as another population with a slightly off-center middle point (Figure 2i, right columns).

3D Plasmonic Tripod Assembly. To fabricate the plasmonic reconfigurable nanomaterial, AuNRs (~12 × 38 nm) were assembled onto the arms of the tripods, forming AuNR-tripods. To minimize cross-binding of AuNRs between tripod arms, three capturing sequences were used for the tripod arms (Figure 3a). AuNRs with corresponding complementary DNA oligos to the capturing strands were incubated with gel-purified tripods, followed by further purification with gel electrophoresis. To examine the binding of AuNRs to the tripod, three sets of AuNRs were added to the tripod in a stepwise manner. Gel electrophoresis showed increasingly retarded mobility of the AuNR-tripods upon sequential adding of three sets of AuNRs (Figures 3b and S5a). Purified constructs were further investigated by TEM, which confirmed the inter-rod angle of 30−30−30, 60−60−60, and 90−90−90 (Figures 3c and S5b). It is worth mentioning that the angles between the AuNRs were distorted in some images due to the deposition of 3D tripods on the 2D TEM grids. Then we performed a reconfiguration experiment on the AuNR-tripods. Figure 3d shows the TEM images of the transformed 30−30−30 AuNR-tripod and the 60−60−60 AuNR-tripod, both converted from the 90−90−90 AuNR-tripod. More studies on transformations, such as the 30−30−30 AuNR-tripod to the 60−60−60 AuNR-tripod conversion and the 60−60−60 AuNR-tripod to the 30−30−30 AuNR-tripod conversion, are demonstrated in Figure S6. AuNRs were also conjugated to asymmetric tripods, 30−90−90, 60−90−90, 30−60−60, and 60−60−90, and purified constructs were confirmed by TEM imaging (Figure S7).

Switching the Plasmonic Property of the AuNR-Tripod. To investigate the conformational effect on the plasmonic property of the AuNR-tripod, we carried out UV−vis spectral analysis. The DNA oligo-coated AuNRs show a longitudinal surface plasmonic resonance (LSPR) peak at 739 nm. While in comparison, the AuNRs in tripod configurations show an 11 nm blue shift, a 6 nm blue shift, a 3 nm red shift, a 1 nm blue shift, a 3 nm blue shift, a 7 nm blue shift, and a 3 nm blue shift for the LSPR peaks of 30−30−30 AuNR-tripod, 60−60−60 AuNR-tripod, 90−90−90 AuNR-tripod, 60−90−90 AuNR-tripod, 30−90−90 AuNR-tripod, 30−60−60 AuNR-tripod, and 60−60−90 AuNR-tripod, respectively (Figure S8a, b). It has been reported earlier that the plasmonic interaction between two AuNRs placed in parallel geometry causes the blue shift of the LSPR peak.[25] After converting the 90−90−90 AuNR-tripod to the 60−60−60 AuNR-tripod and the 30−30−30 AuNR-tripod, the measured LSPR peak shift values were 5 and 8 nm, respectively, toward the blue side of the free AuNR LSPR peak (Figures 3e and S8c,d). These values are in good agreement with the LSPR peaks measured from the preformed 30−30−30 AuNR-tripod and the 60−60−60 AuNR-tripod, also demonstrating the effectiveness of the conformation change fueled by DNA. To further test the reversibility of the reconfiguration of the AuNR-tripods, the 90−90−90 AuNR-tripod was transformed to the 30−30−30 AuNR-tripod back and forth for eight times. The absorbance spectra measured at each step showed the expected change in the LSPR peak (Figures 3f and S9). However, after each conversion, a small red shift and a small blue shift were observed for the 30−30−30 AuNR-tripod and the 90−90−90 AuNR-tripod, respectively. In the final reconfiguration steps, the LSPR peaks at step 8 (the 30−30−30 AuNR-tripod) and Step-9 (the 90−90−90 AuNR-tripod) exhibited a 4 nm red shift and a 5 nm blue shift, in comparison to the LSPR peaks at step 2 (the 30−30−30 AuNR-tripod) and step 1 (the 90−90−90 AuNR-tripod), respectively. The peak shifts are likely due to imperfect conversion efficiency. TEM analysis of the 30−30−30 AuNR-tripod and 90−90−90 AuNR-tripod at steps 8 and 9 confirmed that some AuNR-tripods were subject to incomplete conversion after multiple cycles of transformation (Figure S10).

Single-Structure Dark-Field Scattering Spectroscopy. To investigate the near-field coupling among the three AuNRs, a single-structure dark-field scattering spectroscopy was

DOI: 10.1021/acsnano.6b06861
ACS Nano 2017, 11, 1172−1179

employed. The biotin-modified AuNR-tripod nanostructures (Figure 4a) were deposited on a streptavidin-functionalized

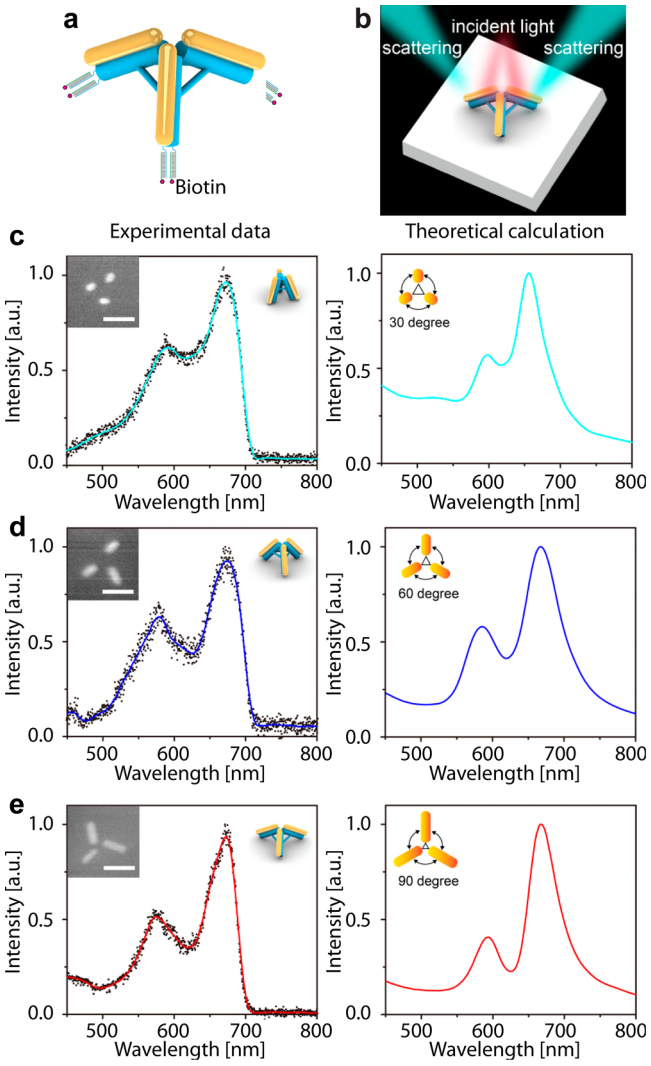


Figure 4. Dark-field scattering spectra of a AuNR-tripod. (a) Schematic diagram of a AuNR-decorated tripod with two biotins on each arm for substrate immobilization with stand-up orientation. (b) Schematic diagram showing assembly of a AuNR-tripod on a silicon wafer for dark-field scattering spectroscopy characterization. (c to e) Experimental scattering spectra (left) and simulated light-scattering spectra (right) for an individual AuNR-tripod with a configuration of 30−30−30 (c), 60−60−60 (d), and 90−90−90 (e). Insets show the SEM images of the AuNR-tripod giving rise to each scattering spectrum. Insets on the right side show the designated configuration for simulation; the size of AuNR is ∼38 nm × 12 nm. Scale bars: 50 nm.

silicon wafer and immobilized by biotin−streptavidin interaction so that they can present the stand-up configuration (Figure 4b) (see Methods for details). DNA-PAINT imaging showed that biotin-modified tripods can be deposited on streptavidin-coated glass slide in a stand-up configuration (Figure 2i). The specificity of the AuNR-tripod attachment to the functionalized wafer surface was confirmed by comparing scanning electron microscopy (SEM) images of the AuNR-tripod with and without biotin modification while deposited onto wafers (Figures S11 and S12). Figures 4c−e and S13 show the scattering spectra of the 30−30−30 AuNR-tripod, the 60−60−60 AuNR-tripod, and the 90−90−90 AuNR-tripod, respectively. All three configurations have two peaks, at ∼570 and ∼650 nm, with a peak split at ∼600 nm. The 90−90−90 AuNR-tripod has a more apparent peak split in comparison to the 30−30−30 AuNR-tripod and the 60−60−60 AuNR-tripod. The relative intensity difference between two peaks becomes gradually more pronounced upon increasing the angles between AuNRs, *i.e.*, changing from 30−30−30 to 90−90−90. According to our design, the gap among the three AuNRs at the vertex of the tripod gradually decreases from the 30−30−30 configuration to the 90−90−90 configuration. As the distance between AuNRs keeps getting shorter, the peak split of the dark-field spectrum becomes more apparent. A theoretical study on the optical response of the AuNR-tripod nanostructures was performed based on mode-coupling analysis and the finite-difference time-domain (FDTD) simulation (see Methods and Supporting Information for more details). Our theory indicates that the near-field coupling among the AuNRs leads to the splitting of the modes and results in hybrid modes (corresponding to the peaks in the dark-field spectrum). The intensification of near-field coupling (with decreasing gap) leads to increase in peak splitting from 30−30−30 to 90−90−90 configuration. Moreover, the main feature of the scattering spectra may be ascribed to the plasmonic analogue of electromagnetically induced transparency,[43,47] which comes from the interference among the fields from bright modes (due to dipole excitation) and dark modes (due to quadrupole excitation). Our experimental results and theoretical calculations agree well qualitatively.

CONCLUSION

We fabricated 3D reconfigurable plasmonic nanostructures regulated by tuning the interarm angles of the DNA origami tripod template *via* toehold-mediated strand displacement reaction. The AuNR-tripod nanostructures could be immobilized onto a substrate through biotin−streptavidin interaction with a stand-up configuration; hence we can precisely control the relative orientation between the AuNR-tripod nanostructures and the incident light. A strong peak split between two peaks was observed on the scattering spectrum measured by single-structure dark-field scattering spectroscopy for AuNR-tripods, with the relative intensity difference between two peaks becoming more pronounced upon increasing the angles between AuNRs. Different geometric configurations of multi-nanorod systems, as exemplified in this report, may lead to tunable extinction wavelength that could potentially be utilized for single-molecule fluorescence enhancement. Moreover, this system could upgrade the complexity of the coupling modes and result in an advanced signal-transition network. The sophisticated coupling modes in such a dynamic plasmonic nanostructure have potential applications in optical signal transmission and modulators. The spatial and temporal control offered by DNA origami nanotechnology provides a strategy for the development of dynamic plasmonic nanostructures for a variety of applications.

METHODS

Design, Preparation, Purification, and Characterization of Tripods. The DNA origami templates are designed using CaDNano. Each of the tripod arms is composed of 14 parallel double helices packed on a honeycomb lattice. Connections at the vertex are formed by the scaffold strand. Angles between two tripod arms are adjusted by adding a supporting strut consisting of two double helices. By

DOI: 10.1021/acsnano.6b06861
ACS Nano 2017, 11, 1172−1179

changing the length of the strut, angles of 30°, 60°, and 90° are achieved. Figures S18–S20 show schematics of 30–30–30, 60–60–60, and 90–90–90 tripod designs, respectively. DNA tripod structures were synthesized by mixing the "staple" strands (purchased from Integrated DNA Technology, Inc.) with a single-stranded scaffold (p7560) in a molar stoichiometric ratio of 10:1 in 1× TE-Mg^{2+} buffer (40 mM Tris, 2 mM EDTA, 12 mM $MgCl_2$, pH 8). The final concentration of the scaffold was adjusted to 10 nM. The mixture was then annealed in a thermocycler from 65 °C to 25 °C over 36 h. Samples were then subjected to gel electrophoresis (1% agarose) in 0.5× TBE(Tris/Borate/EDTA)-Mg^{2+} buffer (45 mM Tris, 45 mM boric acid, 1 mM EDTA, 10 mM $MgCl_2$) for purification and verification. The purified samples are then confirmed with TEM imaging upon staining the samples with 1% uranyl formate for 15 s. The angle distributions were plotted in a histogram after calculating the interarm angles using the software Image-J. To change the conformation of a tripod, first the strut locking strands were released by adding complementary releasing strands in a 10-fold excess to the purified tripod, followed by annealing at 40 °C for 4 h (Figure S1). Then the locking strands corresponding to the desired angle were added followed by annealing at 35 °C for 2 h, then left overnight.

DNA-PAINT Super-resolution Microscopy. DNA-PAINT super-resolution microscopy was performed with a protocol adapted from previous work.[46] In brief, fluorescence imaging was carried out on an inverted Nikon Eclipse Ti microscope (Nikon Instruments) with objective TIRF mode and a Perfect Focus System and collected on an EMCCD camera (iXon DU-897, Andor Technologies) without EM gain option. DNA-PAINT sample preparation was performed in a custom-constructed flow chamber between a piece of coverslip and a glass slide. Biotin-labeled tripod structures were fixed on the surface *via* a biotin–streptavidin–biotin bridge, by serially flowing in BSA (Bovine Serum Albumin)–biotin (1.0 mg/mL), streptavidin (0.5 mg/mL), and biotin-labeled samples. The chamber was filled with imaging buffer of 10 nM Cy3b-labeled imager strand (TATGTAGAT-Cy3b) in buffer B (10 mM Tris-HCl, 10 mM $MgCl_2$, 1 mM EDTA, 0.1% Tween 20, pH 8.0) and then sealed with epoxy before imaging. DNA-PAINT super-resolution movies were recorded with 561 nm laser illumination at 0.5 kW/cm^2 intensity, with a 5 Hz camera frame rate (200 ms per frame) for 10 000 frames.

Assembly of Nanorods to the Tripod. AuNRs were synthesized using a previously published method (see Supporting Information for details).[48] Three different sets of DNA-modified AuNRs were mixed with the purified tripod structure with molar ratio of 5:1 and annealed at 40 °C for 2 h followed by slow shaking for 12 h. The samples were then purified with 1% agarose gel and verified with TEM imaging.

Silicon Wafer Surface Preparation. The method was based on the previous report with some modification.[32] A silicon wafer was cut into smaller pieces of ~0.8 cm by 0.8 cm that fit into a 2 mL tube. The pieces were washed with acetone, ethanol, and ultrapure water in turn three times and cleaned with piranha solution in an ultrasonic cleaner for 15 min. After that, the wafers were washed with ultrapure water and stored in a 2 mL tube for further treatment. First, in a 2 mL tube, 0.8 mg of BSA and 0.4 mg of BSA-biotion (Sigma-Aldrich) were dissolved with 1 mL of 1 × PBS buffer (pH 7.4). A cleaned silicon wafer (the surface was dried by direct nitrogen gas flow) was put in the tube and incubated overnight at 4 °C. After incubation, the silicon wafer was flushed three times with PBS buffer (pH 7.4) to remove free BSA-biotion (the surface should not get dry to avoid denaturing of the proteins). In the next step, the silicon wafer was covered with the NeutrAvidin solution (0.4 mg of NeutrAvidin per 1 mL of PBS buffer) for 2 h at 4 °C. Finally, the wafer was flushed three times with PBS buffer to remove free NeutrAvidin (the surface should not get dry).

Assembly of AuNR-Tripod Constructs on the Silicon Wafer. Each arm of the tripod was designed with two biotin-modified sites for the wafer surface attachment. A 100 μL amount of 5 nM purified AuNR-tripod samples in 0.5× TBE buffer with 10 mM $MgCl_2$ was added to 400 μL of PBS buffer. The NeutrAvidin-modified silicon wafer was covered with the above-mentioned sample solution and incubated for 4 h at 4 °C. Next, the surface was flushed three times with 0.5× TBE buffer with 10 mM $MgCl_2$ in order to remove unbound AuNR-tripod constructs.

Dark-Field Scattering Spectroscopy Measurements. The AuNR-tripod constructs were dispersed on the silicon wafer, and markers were etched in the substrate using electron beam lithography. The etched markers were located and imaged, and the scattering spectra of the assembly around the markers were measured using a dark-field microscope (ZEISS Axio Imager.A2) equipped with a 60× objective. The scattered light was recorded by a spectrograph CCD (Pixis 400, Roper Scientific, PI, USA) to obtain the scattering spectra. It is noted that the excitation light in this setup was not polarized. The AuNR-tripod in which the three AuNRs are arranged at designated angles introduces the possibility of coupling between longitudinal and transverse modes. The SEM images of the same assembly were collected after the dark-field scattering spectra measurements, allowing direct correlation of the shape and arrangement of the assembly with the scattering spectrum.

Theoretical Calculations: Mode-Coupling Analysis and the Finite-Difference Time-Domain Simulation. In the mode-coupling analysis, the longitudinal plasmon of each AuNR is presented as an oscillator. The coupling among the oscillators (plasmons) leads to hybrid modes corresponding to the peaks in the scattering spectra. The FDTD method is applied to simulate the scattering spectrum of the structure with the geometric parameters of AuNRs used in experiments. An average over different incident light polarization has been performed (see Supporting Information for details).

ASSOCIATED CONTENT

Supporting Information

The Supporting Information is available free of charge on the ACS Publications website at DOI: 10.1021/acsnano.6b06861.

Materials and methods, theoretical calculations, supporting figures, and DNA sequences (PDF)

AUTHOR INFORMATION

Corresponding Authors

*E-mail: zhang_wei@iapcm.ac.cn.
*E-mail: dingbq@nanoctr.cn.
*E-mail: yonggang.ke@emory.edu.

ORCID

Yonggang Ke: 0000-0003-1673-2153

Author Contributions

#P. Zhan, P. K. Dutta, and P. Wang contributed equally.

Notes

The authors declare no competing financial interest.

ACKNOWLEDGMENTS

This work is supported by a Wallace H. Coulter Department of Biomedical Engineering Faculty Startup Grant and a Winship Cancer Institute Billi and Bernie Marcus Research Award to Y.K. B.D. acknowledges the support from National Natural Science Foundation of China (21573051, 91127021, 21273052), the National Basic Research Programs of China (2016YFA0201601), the Beijing Natural Science Foundation (L140008), Beijing Municipal Science & Technology Commission (Z161100000116036), and CAS Interdisciplinary Innovation Team. W.Z. acknowledges the support from National Natural Science Foundation of China (11174042, 11374039) and National Basic Research Program of China (973 Program) (2011CB922204, 2013CB632805). P.Y. acknowledges support from National Institutes of Health (1R01EB018659).

DOI: 10.1021/acsnano.6b06861
ACS Nano 2017, 11, 1172–1179

REFERENCES

(1) Boltasseva, A.; Atwater, H. A. Low-Loss Plasmonic Metamaterials. *Science* **2011**, *331*, 290−291.
(2) Luk'yanchuk, B.; Zheludev, N. I.; Maier, S. A.; Halas, N. J.; Nordlander, P.; Giessen, H.; Chong, C. T. The Fano Resonance in Plasmonic Nanostructures and Metamaterials. *Nat. Mater.* **2010**, *9*, 707−715.
(3) Li, W.; Coppens, Z. J.; Besteiro, L. V.; Wang, W. Y.; Govorov, A. O.; Valentine, J. Circularly Polarized Light Detection with Hot Electrons in Chiral Plasmonic Metamaterials. *Nat. Commun.* **2015**, *6*, 8379.
(4) Wurtz, G. A.; Pollard, R.; Hendren, W.; Wiederrecht, G. P.; Gosztola, D. J.; Podolskiy, V. A.; Zayats, A. V. Designed Ultrafast Optical Nonlinearity in a Plasmonic Nanorod Metamaterial Enhanced by Nonlocality. *Nat. Nanotechnol.* **2011**, *6*, 106−110.
(5) Stewart, M. E.; Anderton, C. R.; Thompson, L. B.; Maria, J.; Gray, S. K.; Rogers, J. A.; Nuzzo, R. G. Nanostructured Plasmonic Sensors. *Chem. Rev. (Washington, DC, U. S.)* **2008**, *108*, 494−521.
(6) Rothemund, P. W. K. Folding DNA to Create Nanoscale Shapes and Patterns. *Nature* **2006**, *440*, 297−302.
(7) Kuzuya, A.; Ohya, Y. Nanomechanical Molecular Devices Made of DNA Origami. *Acc. Chem. Res.* **2014**, *47*, 1742−1749.
(8) Douglas, S. M.; Dietz, H.; Liedl, T.; Hogberg, B.; Graf, F.; Shih, W. M. Self-Assembly of DNA into Nanoscale Three-Dimensional Shapes (Vol 459, Pg 414, 2009). *Nature* **2009**, *459*, 1154−1154.
(9) Ke, Y.; Douglas, S. M.; Liu, M. H.; Sharma, J.; Cheng, A. C.; Leung, A.; Liu, Y.; Shih, W. M.; Yan, H. Multilayer DNA Origami Packed on a Square Lattice. *J. Am. Chem. Soc.* **2009**, *131*, 15903−15908.
(10) Andersen, E. S.; Dong, M.; Nielsen, M. M.; Jahn, K.; Subramani, R.; Mamdouh, W.; Golas, M. M.; Sander, B.; Stark, H.; Oliveira, C. L. P.; Pedersen, J. S.; Birkedal, V.; Besenbacher, F.; Gothelf, K. V.; Kjems, J. Self-Assembly of a Nanoscale DNA Box with a Controllable Lid. *Nature* **2009**, *459*, 73−75.
(11) Ke, Y. G.; Sharma, J.; Liu, M. H.; Jahn, K.; Liu, Y.; Yan, H. Scaffolded DNA Origami of a DNA Tetrahedron Molecular Container. *Nano Lett.* **2009**, *9*, 2445−2447.
(12) Han, D.; Pal, S.; Nangreave, J.; Deng, Z.; Liu, Y.; Yan, H. DNA Origami with Complex Curvatures in Three-Dimensional Space. *Science* **2011**, *332*, 342−346.
(13) Iinuma, R.; Ke, Y.; Jungmann, R.; Schlichthaerle, T.; Woehrstein, J. B.; Yin, P. Polyhedra Self-Assembled from DNA Tripods and Characterized with 3d DNA-Paint. *Science* **2014**, *344*, 65−69.
(14) Zhang, F.; Jiang, S. X.; Wu, S. Y.; Li, Y. L.; Mao, C. D.; Liu, Y.; Yan, H. Complex Wireframe DNA Origami Nanostructures with Multi-Arm Junction Vertices. *Nat. Nanotechnol.* **2015**, *10*, 779−784.
(15) Benson, E.; Mohammed, A.; Gardell, J.; Masich, S.; Czeizler, E.; Orponen, P.; Hogberg, B. DNA Rendering of Polyhedral Meshes at the Nanoscale. *Nature* **2015**, *523*, 441−444.
(16) Veneziano, R.; Ratanalert, S.; Zhang, K. M.; Zhang, F.; Yan, H.; Chiu, W.; Bathe, M. Designer Nanoscale DNA Assemblies Programmed from the Top Down. *Science* **2016**, *352*, 1534.
(17) Dutta, P. K.; Varghese, R.; Nangreave, J.; Lin, S.; Yan, H.; Liu, Y. DNA-Directed Artificial Light-Harvesting Antenna. *J. Am. Chem. Soc.* **2011**, *133*, 11985−11993.
(18) Dutta, P. K.; Levenberg, S.; Loskutov, A.; Jun, D.; Saer, R.; Beatty, J. T.; Lin, S.; Liu, Y.; Woodbury, N. W.; Yan, H. A DNA-Directed Light-Harvesting/Reaction Center System. *J. Am. Chem. Soc.* **2014**, *136*, 16618−16625.
(19) Bui, H.; Onodera, C.; Kidwell, C.; Tan, Y.; Graugnard, E.; Kuang, W.; Lee, J.; Knowlton, W. B.; Yurke, B.; Hughes, W. L. Programmable Periodicity of Quantum Dot Arrays with DNA Origami Nanotubes. *Nano Lett.* **2010**, *10*, 3367−3372.
(20) Schreiber, R.; Do, J.; Roller, E. M.; Zhang, T.; Schuller, V. J.; Nickels, P. C.; Feldmann, J.; Liedl, T. Hierarchical Assembly of Metal Nanoparticles, Quantum Dots and Organic Dyes Using DNA Origami Scaffolds. *Nat. Nanotechnol.* **2014**, *9*, 74−78.
(21) Maune, H. T.; Han, S. P.; Barish, R. D.; Bockrath, M.; Goddard, W. A., III; Rothemund, P. W. K.; Winfree, E. Self-Assembly of Carbon Nanotubes into Two-Dimensional Geometries Using DNA Origami Templates. *Nat. Nanotechnol.* **2010**, *5*, 61−66.
(22) Rinker, S.; Ke, Y. G.; Liu, Y.; Chhabra, R.; Yan, H. Self-Assembled DNA Nanostructures for Distance-Dependent Multivalent Ligand-Protein Binding. *Nat. Nanotechnol.* **2008**, *3*, 418−422.
(23) Pal, S.; Deng, Z.; Ding, B.; Yan, H.; Liu, Y. DNA-Origami-Directed Self-Assembly of Discrete Silver-Nanoparticle Architectures. *Angew. Chem., Int. Ed.* **2010**, *49*, 2700−2704.
(24) Ding, B. Q.; Deng, Z. T.; Yan, H.; Cabrini, S.; Zuckermann, R. N.; Bokor, J. Gold Nanoparticle Self-Similar Chain Structure Organized by DNA Origami. *J. Am. Chem. Soc.* **2010**, *132*, 3248−3249.
(25) Pal, S.; Deng, Z. T.; Wang, H. N.; Zou, S. L.; Liu, Y.; Yan, H. DNA Directed Self-Assembly of Anisotropic Plasmonic Nanostructures. *J. Am. Chem. Soc.* **2011**, *133*, 17606−17609.
(26) Urban, M. J.; Dutta, P. K.; Wang, P.; Duan, X.; Shen, X.; Ding, B.; Ke, Y.; Liu, N. Plasmonic Toroidal Metamolecules Assembled by DNA Origami. *J. Am. Chem. Soc.* **2016**, *138*, 5495−5498.
(27) Tian, Y.; Wang, T.; Liu, W. Y.; Xin, H. L.; Li, H. L.; Ke, Y. G.; Shih, W. M.; Gang, O. Prescribed Nanoparticle Cluster Architectures and Low-Dimensional Arrays Built Using Octahedral DNA Origami Frames. *Nat. Nanotechnol.* **2015**, *10*, 637−644.
(28) Liu, W. Y.; Tagawa, M.; Xin, H. L. L.; Wang, T.; Emamy, H.; Li, H. L.; Yager, K. G.; Starr, F. W.; Tkachenko, A. V.; Gang, O. Diamond Family of Nanoparticle Superlattices. *Science* **2016**, *351*, 582−586.
(29) Wang, P. F.; Gaitanaros, S.; Lee, S.; Bathe, M.; Shih, W. M.; Ke, Y. G. Programming Self-Assembly of DNA Origami Honeycomb Two-Dimensional Lattices and Plasmonic Metamaterials. *J. Am. Chem. Soc.* **2016**, *138*, 7733−7740.
(30) Ding, B.; Deng, Z.; Yan, H.; Cabrini, S.; Zuckermann, R. N.; Bokor, J. Gold Nanoparticle Self-Similar Chain Structure Organized by DNA Origami. *J. Am. Chem. Soc.* **2010**, *132*, 3248−3249.
(31) Kuzyk, A.; Schreiber, R.; Fan, Z.; Pardatscher, G.; Roller, E. M.; Hogele, A.; Simmel, F. C.; Govorov, A. O.; Liedl, T. DNA-Based Self-Assembly of Chiral Plasmonic Nanostructures with Tailored Optical Response. *Nature* **2012**, *483*, 311−314.
(32) Schreiber, R.; Luong, N.; Fan, Z.; Kuzyk, A.; Nickels, P. C.; Zhang, T.; Smith, D. M.; Yurke, B.; Kuang, W.; Govorov, A. O.; Liedl, T. Chiral Plasmonic DNA Nanostructures with Switchable Circular Dichroism. *Nat. Commun.* **2013**, *4*, 2948.
(33) Kuzyk, A.; Schreiber, R.; Zhang, H.; Govorov, A. O.; Liedl, T.; Liu, N. Reconfigurable 3d Plasmonic Metamolecules. *Nat. Mater.* **2014**, *13*, 862−866.
(34) Lan, X.; Wang, Q. Self-Assembly of Chiral Plasmonic Nanostructures. *Adv. Mater.* **2016**, *28*, 10499−10507.
(35) Shen, C. Q.; Lan, X.; Lu, X. X.; Meyer, T. A.; Ni, W. H.; Ke, Y. G.; Wang, Q. Site-Specific Surface Functionalization of Gold Nanorods Using DNA Origami Clamps. *J. Am. Chem. Soc.* **2016**, *138*, 1764−1767.
(36) Chen, Z.; Lan, X.; Chiu, Y. C.; Lu, X. X.; Ni, W. H.; Gao, H. W.; Wang, Q. B. Strong Chiroptical Activities in Gold Nanorod Dimers Assembled Using DNA Origami Templates. *ACS Photonics* **2015**, *2*, 392−397.
(37) Lan, X.; Chen, Z.; Dai, G. L.; Lu, X. X.; Ni, W. H.; Wang, Q. B. Bifacial DNA Origami-Directed Discrete, Three-Dimensional, Anisotropic Plasmonic Nanoarchitectures with Tailored Optical Chirality. *J. Am. Chem. Soc.* **2013**, *135*, 11441−11444.
(38) Funston, A. M.; Novo, C.; Davis, T. J.; Mulvaney, P. Plasmon Coupling of Gold Nanorods at Short Distances and in Different Geometries. *Nano Lett.* **2009**, *9*, 1651−1658.
(39) Lan, X.; Lu, X.; Shen, C.; Ke, Y.; Ni, W.; Wang, Q. Au Nanorod Helical Superstructures with Designed Chirality. *J. Am. Chem. Soc.* **2015**, *137*, 457−462.
(40) Zhou, C.; Duan, X. Y.; Liu, N. A Plasmonic Nanorod That Walks on DNA Origami. *Nat. Commun.* **2015**, *6*, 8102.
(41) Ma, W.; Kuang, H.; Xu, L. G.; Ding, L.; Xu, C. L.; Wang, L. B.; Kotov, N. A., Attomolar DNA Detection with Chiral Nanorod Assemblies. *Nat. Commun.* **2013**, *4*.10.1038/ncomms3689

DOI: 10.1021/acsnano.6b06861
ACS Nano 2017, 11, 1172−1179

(42) Yang, S.; Ni, X. J.; Yin, X. B.; Kante, B.; Zhang, P.; Zhu, J.; Wang, Y.; Zhang, X. Feedback-Driven Self-Assembly of Symmetry-Breaking Optical Metamaterials in Solution. *Nat. Nanotechnol.* **2014**, *9*, 1002−1006.
(43) Liu, N.; Langguth, L.; Weiss, T.; Kastel, J.; Fleischhauer, M.; Pfau, T.; Giessen, H. Plasmonic Analogue of Electromagnetically Induced Transparency at the Drude Damping Limit. *Nat. Mater.* **2009**, *8*, 758−762.
(44) Douglas, S. M.; Chou, J. J.; Shih, W. M. DNA-Nanotube-Induced Alignment of Membrane Proteins for Nmr Structure Determination. *Proc. Natl. Acad. Sci. U. S. A.* **2007**, *104*, 6644−6648.
(45) Jungmann, R.; Avendano, M. S.; Woehrstein, J. B.; Dai, M. J.; Shih, W. M.; Yin, P. Multiplexed 3d Cellular Super-Resolution Imaging with DNA-Paint and Exchange-Paint. *Nat. Methods* **2014**, *11*, 313−318.
(46) Dai, M.; Jungmann, R.; Yin, P. Optical Imaging of Individual Biomolecules in Densely Packed Clusters. *Nat. Nanotechnol.* **2016**, *11*, 798.
(47) Zhang, S.; Genov, D. A.; Wang, Y.; Liu, M.; Zhang, X. Plasmon-Induced Transparency in Metamaterials. *Phys. Rev. Lett.* **2008**, *101*, 047401.
(48) Jana, N. R.; Gearheart, L.; Murphy, C. J. Seed-Mediated Growth Approach for Shape-Controlled Synthesis of Spheroidal and Rod-Like Gold Nanoparticles Using a Surfactant Template. *Adv. Mater. (Weinheim, Ger.)* **2001**, *13*, 1389−1393.

DOI: 10.1021/acsnano.6b06861
ACS Nano 2017, 11, 1172−1179